COMPDYN 2015
5th ECCOMAS Thematic Conference on
Computational Methods in Structural Dynamics and Earthquake Engineering
M. Papadrakakis, V. Papadopoulos, V. Plevris (eds.)
Crete Island, Greece, 25–27 May 2015

# EFFECT OF OPENINGS ON NONLINEAR DYNAMIC RESPONSES OF MASONRY INFILLED RC FRAMES

**Y.P. Yuen**[1], **and J.S. Kuang**[2]

[1] Department of Civil Engineering, Bursa Orhangazi Üniversitesi
Bursa, Turkey
e-mail: terry.yuen@bou.edu.tr

[2] Department of Civil and Environmental Engineering, Hong Kong University of Science and Technology
Clear Water Bay, Kowloon, Hong Kong
cejkuang@ust.hk

**Keywords:** Infilled frame; Nonlinear seismic response analysis; Discrete finite element; Unreinforced masonry wall

**Abstract.** *Due to the architectural efficiency of masonry-infilled reinforced concrete frames, the frames are highly common structural forms for buildings. Research on responses of fully infilled RC frames under seismic effects has been active over the last few decades. Nevertheless, the effect of openings in the infills on the nonlinear dynamic responses has seldom been studied. This paper presents a numerical study on the global nonlinear seismic responses of RC frames containing infill walls with three types of openings, namely two-third storey height infills, window-opening infills and door-opening infills. On the basis of the analysis results, it is found that infilled frames with window or door openings exhibit ratchetting phenomena in hysteretic behaviour leading to asymmetric damage and lateral force transfer mechanisms. Furthermore, serious short column phenomenon occurs in the 2/3-storey-height infilled frame structures, in where the central short columns experience serious localised damage resulting significant pinching phenomenon in the hysteretic loops.*

## 1 INTRODUCTION

Masonry infills are widely applied in partition of reinforced concrete frames. Yet, throughout many worldwide devastating earthquakes [1-4], grave damage and catastrophic collapse of the infilled structures occurred time and again on account of altered structural responses of the RC frames containing infill walls. It is well recognized that he structural behaviour of infilled frames and bare frames may differ because the presence of infills, particularly irregularly arranged infills, can significantly alter local stress distributions in the frame members surrounding the infill walls and vary the overall structural dynamic behaviour. Furthermore, the brittle nature of masonry infill materials often lead to severe degradation of the structural hysteretic behaviour and causes localised damage in the adjacent infill wall-braced structural members under reversed cyclic loading. These modifications of structural action can be detrimental to the seismic performance of buildings, resulting in non-reparable damage of the adjacent structural members, jeopardising human lives and property [5].

Over the last few decades, awareness of the deficiency in current design and analysis methods for infilled frames prompted active research on responses of fully infilled RC frames under seismic effects over the last few decades [6-8], while significant progress in understanding their seismic behaviour has been achieved. Nevertheless, the seismic behaviour of RC frame structures containing infill walls with openings has seldom been studied. It has been reported that under seismic excitations the geometrically symmetric RC frame structures containing infill walls with openings can have significant asymmetric damage patterns [9]. Obviously, this asymmetric damage arising from asymmetric loading transfer mechanisms can have implications for the typical capacity design approach.

To understand the effect of openings in the infill walls on the nonlinear dynamic responses, hysteretic behaviour and force transfer mechanisms of infilled frame structures. This paper presents a numerical study on the global nonlinear dynamic responses of masonry infilled RC frames with different type of openings in infills under seismic. Nonlinear response history analyses of the masonry-infilled RC frames under realistic ground motion records are performed to investigate their seismic behaviour. The prototype used in this study is based on a 2-storey RC building frame designed to resist earthquakes with PGA of 0.15g. Four types of masonry-infills configurations: (1) full infills, (2) 2/3-storey-height infills, (3) infills with window openings and (4) infills with door openings are considered. The prototype structures are modelled with advanced discrete-finite element methods.

## 2 PROTOTYPE STRUCTURES

The prototype structure is a two-storey RC building frame designed to resist earthquakes with a PGA of 0.15g. Confining transverse reinforcement is provided in the frame members, which are detailed to obtain an expected displacement ductility factor of 2 to 4 [10]. The uniaxial strengths of the concrete and longitudinal and transverse reinforcements are 20.1 MPa, 400 MPa and 235 MPa, respectively. The full height 125-mm-thick infill panels are composed of 600×300×125-mm masonry units (compressive strength = 15 MPa) and 10-mm-thick mortar joints (compressive strength = 5 MPa). The reinforcement details and elevation view of the prototype frame is shown in Figure 1. In addition to the full height infills, three typical types of masonry-infill arrangement containing openings are considered in this study: (1) 2/3-storey-height infills, (2) infills with window openings and (3) infills with door openings. The window size is 900 mm square, with two windows in each wall. The windows are located at 2/3 height (from bottom to top) of the wall and 1/3 width (from left to right) of the wall. The door size is 900×2100 mm, with one door in each wall. The door is located in the middle-bottom of the wall.

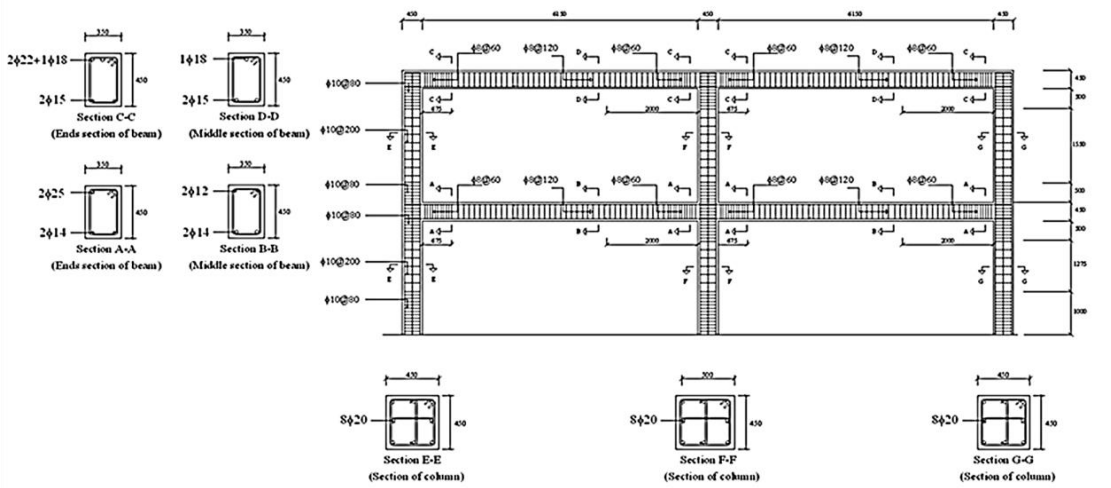


Figure 1: Prototype frame structure.

## 3 DISCRETE FINITE ELEMENT MODELS

To adequately capture the local infill-frame interacting behaviour, detailed modelling and discretisation of the frame and infill components are required. The prototype structures are modelled with advanced discrete-finite element methods are constructed with ABAQUS [11] and the mechanical behaviour of concrete and steel-reinforcement elements are modelled with the smeared isotropic damage-plasticity model [12] and Modified Menegotto-Pinto model [13] respectively. Furthermore, to simulate the pre- and post-fracture behaviour of the mortar joints in the infills, damage-based cohesive interactions [14] are enforced on the contact surfaces of the masonry units. The formulation of the interfacial constitutive model for the mortar joints is briefly outlined below.

As the strength of mortar joints is often much weaker than that of masonry units in infill walls, damage and cracks will likely propagate along the joints. In computational modelling, inelastic deformation will thus be concentrated in the mortar joints with severe distortion of the elements that may impair the accuracy of the simulation. In view of this, the contact formulation is a more effective tool to simulate extended crack opening and propagation behaviour as well as component disintegration in infills. The incremental form of the traction-separation law for cohesive cracks considering the mixed-mode fracture behaviour of the mortar joints is given by

$$\begin{Bmatrix} \Delta t_n \\ \Delta t_s \\ \Delta t_t \end{Bmatrix} = \begin{bmatrix} k_{nn}(1-D\cdot H(t_n)) & 0 & 0 \\ 0 & k_s(1-D) & 0 \\ 0 & 0 & k_t(1-D)) \end{bmatrix} \begin{Bmatrix} \Delta u_n \\ \Delta u_s \\ \Delta u_t \end{Bmatrix} \tag{1}$$

where $\mathrm{t} = \{t_n, t_s, t_t\}$ and $[\mathrm{u}] = \{u_n, u_s, u_t\}$ are the traction and displacement jump vector between two masonry unit surfaces, respectively, and $\mathbf{k_e}$ is an initial isotropic elastic stiffness tensor. The damage variable $D$ is a scalar parameter of value within [0,1], and normal stiffness is assumed to be completely recovered under the compressive normal traction to account for the unilateral effect. $H(t_n)$ is a step function: $H(a)=1$ if $a \geq 0$, otherwise $H(a)=0$, which is used to characterise the unilateral effect or stiffness recovery effect. Due to the ma-

sonry units' restraint, the macroscopic cracks, which inflict macroscopic stiffness degradation, in mortar joints are eventually aligned with the bed planes regardless of fracture modes. By considering the major macroscopic damage mechanism and typical structural actions experienced by infills, it is sufficient to use a damage variable to model the stiffness degradation effect due to the formation of cracks in mortar joints. The criterion of damage initiation is defined as

$$t_n^2 + \beta_s^2 t_s^2 + \beta_t^2 t_t^2 - f_{nt}^2 = 0 \qquad (t_n \geq 0) \tag{2}$$

$$\beta_s^2 (|t_s| + t_n \tan\phi_s)^2 + \beta_t^2 (|t_t| + t_n \tan\phi_t)^2 - f_{nt}^2 = 0 \qquad (t_n < 0) \tag{3}$$

where $f_{nt}$ is the tensile strength of the mortar joints; $\beta_s$ and $\beta_t$ are the ratios of the tensile strength to the mode II shear cohesion strength $c_s$ and mode III tear cohesion strength $c_t$, respectively; and $\phi_s$ and $\phi_t$ are the friction angles under mode II and mode III deformation, respectively. The crack-driving force $G_T$ is defined as

$$\Delta G_T = \{t_n\}\Delta\tau[u_n] + (|t_s| - \{-t_n\}\tan\phi_s)\Delta[u_s] + (|t_t| - \{-t_n\}\tan\phi_t)\Delta[u_t] \tag{4}$$

where $\{\bullet\}$ denotes the Macaulay bracket: $\{a\} = a$ if $a \geq 0$, otherwise $\{a\} = 0$.

It is assumed that the critical strain-energy release rate $G_c$ under mixed-mode fracture is represented [15] as

$$\Delta G_C = -m(G_{IIC} + G_{IIIC} - G_{IC})\left(\frac{G_{IIC} + G_{IIIC}}{G_T}\right)^m G_T \Delta G_T \tag{5}$$

where $G_{IC}$, $G_{IIC}$, and $G_{IIIC}$ are critical strain-energy release rates under pure mode I, pure mode II, and mode III fracture, respectively; $m$ is an exponent that depends on the brittleness of the material; and $G_0$ is the strain-energy release rate at damage initiation. The mixed-mode fraction criterion BK law was developed and verified for ductile and brittle polymer materials, which have amorphous and polycrystalline solid structures, respectively. Hence, the fraction criterion is suitable for a wide range of materials with different molecular or grain structures. The evolution of damage is presented in the form of

$$\Delta D = \max\left(\frac{\Delta G_T}{G_C - G_0} - \frac{G_T \Delta G_C}{(G_C - G_0)^2}, 0\right) \tag{6}$$

When the contact surfaces are under compression, the joints behave similarly to Mohr-Coulomb materials, and crack propagation is governed by mode II fracture. However, when the surfaces are subjected to interacting tension and shear, a mixed-mode fracture criterion of the BK form would control the crack propagation. Once the mortar joints are fractured, $D = 1$, and the post-cracking interaction property of the two contact surfaces follows Coulomb's friction law; thus the slip criterion is defined as

$$f = (|t_s| - \{-t_n\}\tan\phi_s)^2 + (|t_t| - \{-t_n\}\tan\phi_t)^2 = 0 \tag{7}$$

The friction force is treated as constant, i.e., the change is zero at each time increment under the explicit Euler integration scheme, and the possible change in friction force is accounted at the end of integration. The model II or mode III fracture energy presented here is the macroscopically averaged energy, minus the frictional dissipation under normal compression, required for shearing masonry composites to failure or fracture states. Thus frictions are sub-

tracted from the total shear tractions in Eq. 6, and when a certain part of the strain energy is completely released due to fracture $D = 1$, the frictional dissipation dictated by Coulomb's law (Eq. 7) can continue. Hence, a smooth transition from the traction-separation law to Coulomb's law is attained.

The model is implemented in ABAQUS through the user-subroutine VUINTERACTION for traction-separation behaviour in general contact simulations. The integration scheme used for the implementation of the model is based on a standard modified explicit Euler scheme with substepping [16]. To illustrate the numerical algorithms of the model implementation, the solution steps for the mortar joints stressed from the elastic state to the damaged state, which are similar for other states, are outlined in Figure 2.

1. At a integration point on a contact surface, start with $\mathbf{t}^n$, $[\mathbf{u}^n]$, $D^n$, $G_c{}^n$, $G_T{}^n$, $\mathbf{k_e}$ and $\Delta[\mathbf{u}^{n+1}]$.
2. Check if the mortar joints fractured ($D^n = 1$)? If fractured, go subroutine to integrate the Columb friction problem.
3. Check if the mortar joints damaged ($D^n > 0$)? If damaged, go to step 8 with $\tau = 0$ and $\Delta\tau = 1$, $G_T^0 = G_T^n$, $G_c^0 = G_c^n$ and $\Delta[\mathbf{u}]_d = \Delta[\mathbf{u}^{n+1}]$.
4. Calculate elastic predictor: $\mathbf{t_e} = \mathbf{t}^n + \mathbf{k_e}\Delta[\mathbf{u}^{n+1}]$ and

$$F = \left\langle t_n^{n+1} \right\rangle^2 + \beta_s^2 \left\langle t_s^{n+1} \right\rangle^2 + \beta_t^2 \left\langle t_t^{n+1} \right\rangle^2 - f_{nt}^2 \qquad (t_n^{n+1} \geq 0)$$

$$F = \beta_s^2 \left\langle t_s^{n+1} \right| + t_n^{n+1} \tan\phi_s \left\rangle^2 + \beta_t^2 \left\langle t_t^{n+1} \right| + t_n^{n+1} \tan\phi_s \left\rangle^2 - f_{nt}^2 \qquad (t_n^{n+1} < 0)$$

5. If $F \leq 0$, then $\mathbf{t}^{n+1} = \mathbf{t_e}$ and exit
6. If $F > 0$, calculate portion of $\Delta[\mathbf{u}^{n+1}]$ that cause purely elastic deformation, $\alpha$, using the modified regula-falsi intersection scheme. Set $\mathbf{t}^0 = \mathbf{t}^n + \mathbf{k_e}\,\alpha\,\Delta[\mathbf{u}^{n+1}]$ and

$$G_0 = G_T^n + \left\{ \begin{matrix} \langle t_n^{(n+1)/2} \rangle \\ \left| t_s^{(n+1)/2} \right| + \left\{ -t_n^{(n+1)/2} \right\} \tan\phi_s \\ \left| t_t^{(n+1)/2} \right| + \left\{ -t_n^{(n+1)/2} \right\} \tan\phi_t \end{matrix} \right\} \alpha\Delta \left[ \begin{matrix} u_n^{n+1} \\ u_s^{n+1} \\ u_t^{n+1} \end{matrix} \right] \quad \text{where } \mathbf{t}^{(n+1)/2} = (\mathbf{t_0} + \mathbf{t}^n)/2$$

7. Set $\tau = 0$ and $\Delta\tau = 1$, $G_T^0 = G_0$, $G_C^0 = G_C^n$ and $\Delta[\mathbf{u}]_d = (1-\alpha)\,\Delta[\mathbf{u}^{n+1}]$
8. While $\tau < 0$, do steps 9 to 14
9. For $i = 1,2$, calculate

$$\Delta t^i = (\mathbf{I} - D^i \mathbf{S})\mathbf{k}_e \Delta\tau \Delta[\mathbf{u}]_d$$

$$\Delta G_T^i = \left\{ \begin{matrix} \langle t_n^i \rangle \\ \left| t_s^i \right| - \left\{ -t_n^i \right\} \tan\phi_s \\ \left| t_t^i \right| - \left\{ -t_n^i \right\} \tan\phi_t \end{matrix} \right\} \Delta\tau \left[ \begin{matrix} u_n \\ u_s \\ u_t \end{matrix} \right]_d$$

$$\Delta G_C^i = -m(G_{IIC} + G_{IIIC} - G_{IC}) \left( \frac{G_{IIC} + G_{IIIC}}{G_T^i} \right)^m G_T^i \Delta G_T^i \qquad \Delta D^i = \max\left( \frac{\Delta G_T^i}{G_C^i - G_0} - \frac{G_T^i \Delta G_C^i}{(G_C^i - G_0)^2}, 0 \right)$$

where $\mathbf{S} = \begin{bmatrix} H(t_n^i) & 0 & 0 \\ 0 & 1 & 0 \\ 0 & 0 & 1 \end{bmatrix}$ is matrix used to characterise unilateral effect and

$$\mathbf{t}^1 = \mathbf{t}^\tau, \quad D^1 = D^\tau, \quad G_T^1 = G_T^\tau, \quad G_C^1 = G_C^\tau$$

$$\mathbf{t}^2 = \mathbf{t}^\tau + \Delta\mathbf{t}^1, \quad D^2 = D^\tau + \Delta D^1, \quad G_T^2 = G_T^\tau + \Delta G_T^1, \quad G_C^2 = G_C^\tau + \Delta G_C^1$$

10. Compute the new traction vector, damage variable and strain energy releases rates as

$$\Delta\mathbf{t}^{\tau+\Delta\tau} = \mathbf{t}^\tau + \frac{1}{2}\left(\Delta\mathbf{t}^1 + \Delta\mathbf{t}^2\right), \qquad \Delta D^{\tau+\Delta\tau} = D^\tau + \frac{1}{2}\left(\Delta D^1 + \Delta D^2\right)$$

$$\Delta G_T^{\tau+\Delta\tau} = G_T^\tau + \frac{1}{2}\left(\Delta G_T^1 + \Delta G_T^2\right), \quad \Delta G_C^{\tau+\Delta\tau} = G_C^\tau + \frac{1}{2}\left(\Delta G_C^1 + \Delta G_C^2\right)$$

11. Determine the relative error as

$$R^{\tau+\Delta\tau} = \max_i \left\{ \frac{\left\| \Delta\xi_i^2 - \Delta\xi_i^1 \right\|}{\left\| \Delta\xi_i^{\tau+\Delta\tau} \right\|} \right\}$$ where $\xi$ is a set of all calculated state variables from the previous step.

12. If $R^{\tau+\Delta\tau} \geq TOL$ then go to step 9 with a smaller pseudo-time increment

$$\Delta\tau = \max(0.9\sqrt{TOL/R^{\tau+\Delta\tau}}\,\Delta\tau, 0.1\Delta\tau, \Delta\tau_{\min})$$

13. If $R^{\tau+\Delta\tau} < TOL$ (solution tolerance)

$$\mathbf{t}^{\tau+\Delta\tau} = \mathbf{t}^\tau + \Delta\mathbf{t}^{\tau+1}, \qquad D^{\tau+\Delta\tau} = D^\tau + \Delta D^{\tau+\Delta\tau} \qquad G_T^{\tau+\Delta\tau} = G_T^\tau + \Delta G_T^{\tau+\Delta\tau},$$

$$G_C^{\tau+\Delta\tau} = G_C^\tau + \Delta G_C^{\tau+\Delta\tau}$$

14. Extrapolate to obtain the pseudo-time increment of the next sub-step by

$$\Delta\tau = \min(0.9\sqrt{TOL/R^{\tau+\Delta\tau}}\,\Delta\tau, \Delta\tau, 1-\Delta\tau) \quad \tau = \tau + \Delta\tau$$

15. When $\tau = 1$, exit with

$$\mathbf{t}^{n+1} = \mathbf{t}^1, \quad D^{n+1} = D^1, \quad G_T^{n+1} = G_T^1, \quad G_C^{n+1} = G_C^1$$

Figure 2: Solution steps for the mortar joints stressed from elastic state to damaged state.

## 4 SEISMIC FAILURE MODES AND FORCE TRANSFER MECHANISMS

Each of the infilled frame structures are subjected to four real earthquake ground motions: (1) 1979 El Centro 1140-component at USGS-station 5056 (PGA = 0.14g), (2) 1987 Superstition Hills 225-component at USGS-station 5051 (PGA = 0.46g), (3) 1995 Kobe 000-component at station Takatori (PGA = 0.61g) and (4) 1999 Chi-Chi EW-component at station CHY080 (PGA = 0.96g). The elastic response spectra of the four ground motions are shown in Figure 3.

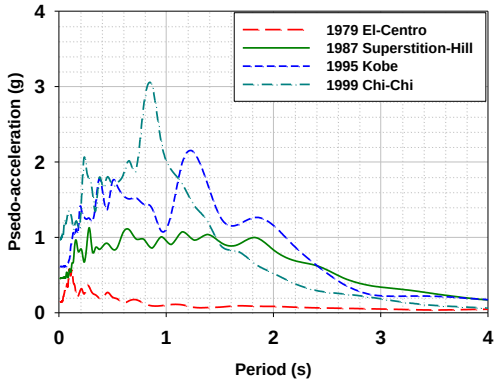


Figure 3: Elastic response spectra of the ground motions.

Under the four ground excitations, the resulted hysteresis loops of the prototype structures are plotted in Figure 4. Comparing with the frames with full-height solid infills, the introduction of openings in the infill panels significantly reduces the incurred bracing action against the bounding frame. The maximum base shears experienced by the infilled frames with window openings are reduced to approximately two-thirds to as much as one-half of that experienced by the fully infilled frames; surprisingly, the damage to the bounding RC frame and the infill panel is the most severe amongst the four infilled structures, as shown in Figure 5. Yet, the structure is still able to attain higher lateral stability than the frame with captive columns, as shown in Figure 4.

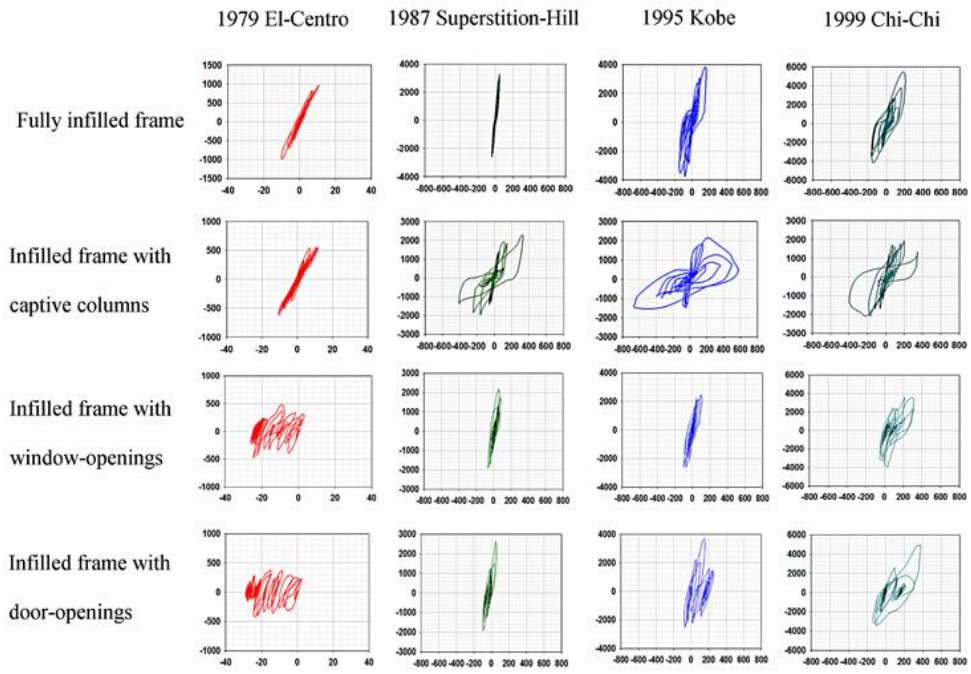


Figure 4: Hysteresis behaviour of infilled frames

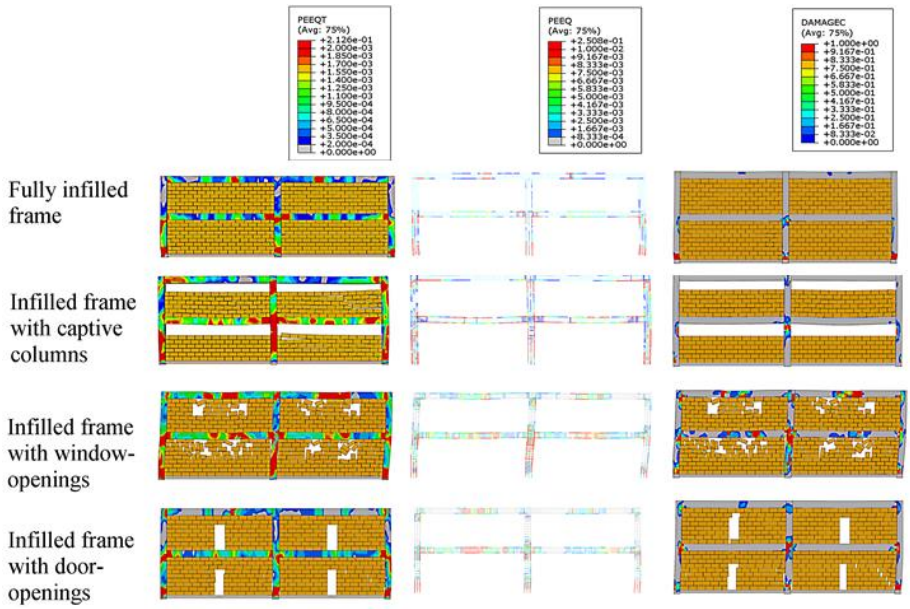


Figure 5: Damage pattern of infilled frames.

Although the incurred seismic forces are quite significantly reduced by the introduction of openings, very serious damage that is much more severe than that inflicted upon the fully infilled frames subjected to higher seismic forces is inflicted on the bounding RC frame under seismic loading. This apparently abnormal behaviour is due to the partial collapse of the holed infill panels, as shown in Figure 5. Stored strain energy in the collapsing infill components is suddenly released, resulting in severe, localised damage to the infill. In other words, following the toppling of infills, most of the seismic vibration energy is absorbed by the bounding frames rather than the infills in infilled frame structures with window openings, in contrast to the fully infilled frames, in which most of the vibration energy is apparently absorbed by the non-toppled infills.

Nevertheless, the infilled frames with window openings can attain quite reasonable post-damage lateral stability, although the structures suffer more extensive damage than other infilled frames. Again, the vertical and lateral bracing actions provided by the full-height infill panels contribute this stability to the structure. This result demonstrates the importance of the continuity of the infill distribution in a bounding frame to the global stability of the structure. A discontinuous infill distribution, such as the infilled frames with captive columns, tends to have lower post-damage lateral stability because any force-flow discontinuity can prohibit the development of other force transfer mechanisms, decreasing the potential for force redistribution. Therefore, even with such severe damage being inflicted on the structure, the continuous non-toppled infills in the infilled frames with window openings are still able to transmit the lateral and vertical forces through multiple strut bracing mechanisms, as shown in Figure 6.

By contrast, while other frames behave elastically under the 1979 El Centro earthquake, the infilled frames with openings exhibit a ratchetting phenomenon in which the irrecoverable inelastic drift develops progressively with each loading cyclic, as shown in Figure 4, quite similar to the fatigue effect. This phenomenon occurs because the cracking strength of the infill panels with openings is lower than that of solid infills due to stress concentration in the corners, as shown in Figure 6. As a result, sliding cracks are initiated at those corners and progressively propagate along the bed joints under cyclic loadings, and the inelastically deformed infill panels restrain the undamaged bounding frame from deflecting back to the original configuration, resulting in the development of residual drift.

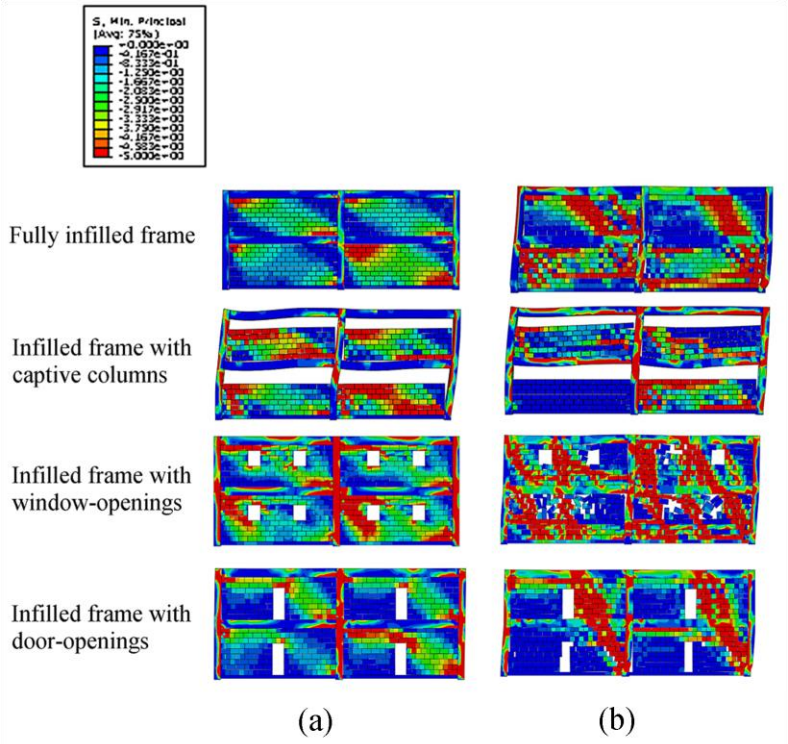


Figure 6: Force transfer mechanisms: plots of the principal compressive stress distribution of infilled frames (a) before major cracking and (b) after major cracking.

Similar to window openings, door openings weaken the bracing action of infills to the bounding frame. The incurred base shear is reduced to approximately 80%, as much as 50% of that experienced by the fully infilled frames. As shown in Figure 5, the structures exhibit rather asymmetrical damage patterns; the rightmost columns suffer more severe damage than the leftmost columns, while opposite damage distributions are evident in the beams, which more damage is inflicted in the left beams. Although the infilled frames with door openings exhibit lower initial stiffness and thus experience less seismic forces than the structures with window openings under the excitation of the El Centro earthquake, the post-damage stiffness and base shear of the former structures become considerably larger than that of the later structures under the other three strong earthquake excitations. This increase can be understood by observing the initial and post-damaged force transfer mechanisms, as shown in Figure 6.

The "door" structures have weaker initial bracing action than the "window" structures, but after the infills suffer severe damage with the formation of major cracks or even partially collapse, the post-damaged lateral bracing mechanisms, as characterised by the inclined compressive struts, of the "door" structures are much stronger and more robust than the "window" structures. As a result, the incurred base shears of the "door" structures are larger in the post-damage states and can reach magnitudes as high as 80% of that experienced by the fully infilled frames. The structural damage of the frames with door openings is less than that incurred on the frames with window openings due to reduced disintegration of infill components.

However, the damage is apparently more severe than that to the fully infilled frames, or more precisely speaking, the damage distribution is considerably asymmetric, as indicated previously. This increase in severity occurs because the initially symmetric lateral force transfer mechanisms are destroyed by the ratchetting effect. In contrast to the "window" structures, the infills founded on the floors in the "door" structures are not horizontally continuous

due to the introduction of the door openings, which results in unrestrained sliding of the infill panels. Sliding of the infill panels leads to strong variation of the lateral force transfer mechanisms, as well as the resulting drifts and hysteresis loops, of the structures under loading acting in two opposite directions. Although the lateral stability remains quite satisfactory for the prototype structure with door openings adopted in this study, if the structures were taller, the stability would decrease because a significant P-Δ effect would be triggered under large vertical loading and lateral drift.

## 5 CONCLUSIONS

On the basis of the analysis results, the following conclusions are drawn:

- Non-toppled full infills panels can enhance the overall stability and energy dissipation, though the structures suffer much larger seismic forces.
- Infilled frames with window or door openings exhibit, respectively, shakedown or ratchetting phenomena in hysteretic behaviour due to the propagation of sliding cracks initiated from the corners of the openings.
- Unrestrained ratchetting deformation in the infilled frames with door openings incur serious asymmetric damage patterns and lateral force transfer mechanisms.
- Serious short column phenomenon occurs in the 2/3-storey-height infilled frame structures, in where the central short columns experience serious localised damage and this leads to significant pinching phenomenon in the hysteretic loops.

## ACKNOWLEDGMENT

The support of Hong Kong Research Grant Council under grant No. 614011 and Scientific and Technological Research Council of Turkey (TÜBİTAK) under project number 214M236 are gratefully acknowledged.

## REFERENCES

[1] H. Sezen, A. S. Whittaker, K. J. Elwood, K. M. Mosalam. Performance of reinforced concrete buildings during the August 17, 1999 Kocaeli, Turkey earthquake, and seismic design and construction practise in Turkey. *Engineering Structures*, **25**, 103-114, 2003.

[2] Earthquake Engineering Field Investigation Team (EEFIT). *The 2007 August 15 magnitude 7.9 earthquake near the coast of Central Peru*. The Institution of Structural Engineers, UK, 2007.

[3] Earthquake Engineering Field Investigation Team (EEFIT). *The Wenchuan, China earthquake of 12 May 2008*. The Institution of Structural Engineers, UK, 2008.

[4] M. Manfredi, A. Prota, G. M. Verderame, F. De Luca, P. Ricci. 2012 Emilia earthquake, Italy: reinforced concrete buildings responses. *Bulletin of Earthquake Engineering*, **12**, 2275-2298, 2014.

[5] T. Paulay, M. J. N. Priestley. *Seismic design of reinforced concrete and masonry buildings*. Wiley, New York, 1992.

[6] A. B. Mehrabi, P. B. Shing. Behaviour and analysis of masonry-infilled frames. *Progress in Structural Engineering and Materials*, **4**(3), 320-331, 2002.

[7] P. Ricci, M. T. De Risi, G. M. Verderame, G. Manfredi. Influence of infill distribution and design typology on seismic performance of low- and mid-rise RC buildings. *Bulletin of Earthquake Engineering*, **11**, 1585-1616, 2013.

[8] F. De Luca, G. M. Verderame, F. Gómez-Martínez, A. Pérez-García. The structural role played by masonry infills on RC building performances after the 2011 Lorca, Spain, earthquake. *Bulletin of Earthquake Engineering*, **12**, 1999-2026, 2014.

[9] D. J. Kakaletsis, C. G. Karayannis. Influence of masonry strength and openings on infilled R/C frames under cycling loading. *Journal of Earthquake Engineering*, **12**(2), 197-221, 2008.

[10] SAC. *Code for seismic design of buildings: GB 50011-2001*. China Architecture & Building Press, Beijing, 2001.

[11] ABAQUS, Inc. *ABAQUS theory manual*, 2010.

[12] J. Lubliner, J. Oliver, S. Oller, E. Oñate, A plastic-damage model for concrete. *International Journal of Solids and Structures*, **25**, 229–326, 1989.

[13] J. Sakai, K. Kawashima, Modification of the Giuffre, Menegotto and Pinto Model for unloading and reloading paths with small strain variations. *Journal of Structural Mechanics and Earthquake Engineering*, **738/I-64**, 159–169, 2003.

[14] J. S. Kuang, Y. P. Yuen, Simulations of masonry-infilled RC frames failure. *Engineering and Computational Mechanics, ICE*, **166**, 179-193, 2013.

[15] M. L. Benzeggagh, M. Kenanem. Measurement of mixed-mode delamination fracture toughness of unidirectional glass/epoxy composites with mixed-mode bending apparatus. *Composites Science and Technology*, **56**(4), 439–44 9, 1996.

[16] S. W. Sloan, A. J. Abbo, D. Sheng. Refined explicit integration of elastoplastic models with automatic error control. *Engineering Computations*, **18**(1/2), 121-154, 2001.